Although $HSiO^-$ will not transfer a hydride to acetone (HA = 39.6 kcal mol^{-1}), acetaldehyde (HA = 40.7 kcal mol^{-1}), or benzaldehyde (HA = 45.9 kcal mol^{-1}), hydride transfer to acrylonitrile (HA = 57.6 kcal mol^{-1}) and acrolein (HA = 61.5 kcal mol^{-1}) is observed. Hydride transfer to CO_2 (HA = 51.6 kcal mol^{-1}) leads to an ion of mass 45, the same mass as $HSiO^-$; however, experiments with $^{13}CO_2$ resulted in an ion of mass 46 ($H^{13}CO_2^-$) indicating hydride transfer. Therefore, the hydride affinity of SiO is somewhere between that of CO_2 and benzaldehyde and may be assigned a value of 49 ± 5 kcal mol^{-1}. By eq 23, the $\Delta H°_f$ ($HSiO^-$) is determined to be −38 ± 5 kcal mol^{-1}.

$$\Delta H°_f(HSiO^-) = -HA(SiO) + \Delta H°_f(SiO) + \Delta H°_f(H^-) \quad (23)$$

It is interesting to compare the hydride affinity of SiO (HA = 49 kcal mol^{-1}) with that of the isoelectronic carbon analogue, CO (HA = 8 kcal mol^{-1}). Although the hydride in HCO^- is barely bound, the hydride in $HSiO^-$ is bound more strongly than those in simple alkoxides such as $CH_3CH_2O^-$ (HA = 40.7 kcal mol^{-1}). This gives evidence of the clear difference between C=O and Si=O species. Obviously, SiO is much more willing than CO to accept the hydride at the expense of a π-bond to oxygen.

It also is possible to bracket the proton affinity of the $HSiO^-$ anion and, as a result, determine the heat of formation of its parent (H_2SiO or HSiOH).[29] This procedure is complicated because we have a minor H_3SiO^- contamination, and $HSiO^-$ reacts with standard acids in ways other than proton transfer. Proton abstraction from acetic acid ($\Delta G°_{acid}$ = 341 kcal mol^{-1}), cyclopentadiene (ΔG_{acid} = 348 kcal mol^{-1}), and nitromethane ($\Delta G°_{acid}$ = 350 kcal mol^{-1}) is observed, and a lower limit of 350 kcal mol^{-1} can be placed on the acidity of the parent compound. Because $HSiO^-$ does not react with acetone, we can set an upper limit of 362 kcal mol^{-1} on its acidity. Reactions with compounds of intermediate acidity led to inconclusive results; therefore, we must report the proton affinity of $HSiO^-$, $\Delta G°_{acid}$ = 356 ± 8 kcal mol^{-1} with large error bars. Taking the proton affinity and the heat of formation of $HSiO^-$, the heat of formation of H_2SiO (HSiOH) may be estimated with eq 24.[30] The value obtained in this way,

$$\Delta H°_f(H_2SiO, HSiOH) = \Delta H°_f(HSiO^-) + \Delta H°_f(H^+) - \Delta H°_{acid}(HSiO^-) \quad (24)$$

$\Delta H°_f(H_2SiO, HSiOH)$ = −36 ± 10 kcal mol^{-1}, corresponds to the heat of formation of the more stable isomer assuming that protonation at silicon and oxygen are both kinetically viable.

Acknowledgment. We gratefully acknowledge support of this research by the National Science Foundation under Grants CHE-8615808 (R.D.) and CHE-8815459 (C.H.D.). In addition, C.H.D. acknowledges the Alexander von Humboldt-Stiftung for a Senior U.S. Scientist Award and the Institut für Organische Chemie der Technischen Universität Berlin for hospitality while part of this work was accomplished.

(28) Hydride affinities are taken from a compiliation provided by Squires, R. R., Purdue University. See: Hajdasz, D. J.; Squires, R. R. *J. Am. Chem. Soc.* **1986**, *108*, 3139.

(29) Proton affinities and heats of formation of anions are taken from the following: Lias, S. G.; Bartmess, J. E.; Liebman, J. F.; Holmes, J. L.; Levin, R. D.; Mallard, W. G. *J. Phys. Chem. Ref. Data* **1988**, *17*, Supplement No. 1.

(30) The free energy of protonation may be converted to an enthalpy by estimating the entropy of protonation, see: Bartmess, J. E.; McIver, R. T., Jr. In *Gas Phase Ion Chemistry*; Bowers, M. T., Ed., Academic Press: New York, 1979; Vol. 2.

Subpicosecond Fluorescence Anisotropy Studies of Tryptophan in Water

Anthony J. Ruggiero, David C. Todd,† and Graham R. Fleming*

Contribution from the Department of Chemistry, the Department of Physics, and The James Franck Institute, The University of Chicago, 5735 South Ellis Avenue, Chicago, Illinois 60637.
Received May 19, 1989

Abstract: Ultraviolet fluorescence upconversion optical gating has been used to measure the excitation and emission wavelength dependence of the fluorescence depolarization of tryptophan in water with subpicosecond resolution. An initial anisotropy of 0.4 is observed for the first time. The short time decay behavior is found to be complicated by non-rotational contributions to the anisotropy decay arising from the interaction of the two low-lying ^1L_a and ^1L_b excited states. The time constant for ^1L_b to ^1L_a internal conversion is found to be 1.6 ± 0.2 ps. A generalized version of the level kinetics model of Cross et al.[29] is found to adequately describe the fluorescence anisotropy decay dependence on excitation and emission wavelength. The anisotropy data are interpreted in terms of a model for tryptophan fluorescence depolarization that includes the effects of vibronic coupling and vibrational relaxation. Our results indicate that the fluorescence anisotropy will be an ambiguous method of studying protein motion for times less than 5–10 ps.

For more than three decades, the electronic spectroscopy and photophysics of tryptophan and its derivatives in solution have been the subject of intense study.[1-3] This effort has been motivated by the desire to understand the near-ultraviolet absorption and fluorescence properties of tryptophanyl residues in proteins and establish a basis for their use as intrinsic probes of protein structure and conformational dynamics.[4-7] An accurate characterization of the short time fluorescence anisotropy behavior of tryptophan has become particularly important. Molecular dynamics simulations of small proteins have suggested that sig-

* Address correspondence to this author at the Department of Chemistry.
† Department of Physics.

(1) Creed, D. *Photochem. Photobiol.* **1984**, *39*, 537.
(2) Konev, S. V. *Fluorescence and Phosphorescence of Proteins and Nucleic Acids*; Plenum: New York, 1967.
(3) Longworth, J. W. In *Excited States of Proteins and Nucleic Acids*; Steiner, R. F., Weinryb, I., Eds.; Plenum: London, 1971; p 319.
(4) Longworth, J. W. In *Time-Resolved Fluorescence Spectroscopy in Biochemistry and Biology*; Cundall, R. B., Dale, R. E., Eds.; Plenum: London, 1983.
(5) Beechem, J. M.; Brand, L. *Annu. Rev. Biochem.* **1985**, *54*, 43.

0002-7863/90/1512-1003$02.50/0

nificant internal motion takes place on the picosecond and subpicosecond time scale.[8-11] These thermally driven conformational fluctuations are believed to play a crucial role in determining the physical properties and biological functions of many proteins.[12,13] The measurement of the fluorescence anisotropy decay of tryptophanyl residues is one of the few experimental approaches available that can provide information on both the rate and amplitude of this type of internal mobility. Time-resolved fluorescence depolarization measurements depend directly on the decay of the time correlation function for the reorientation of molecular absorption and emission transition dipole moment vectors.[14,15] In principle, the fluorescence depolarization technique should permit a detailed description of the reorientational motion of the tryptophan chromophore and a direct comparison of theory and experiment over the few-hundred picosecond period currently accessible by computer simulation.

Unfortunately, the spectroscopy of tryptophan is complicated by the existence of two overlapping electronic transitions in the 250–300 nm region, designated the ^1L_a and ^1L_b transitions.[16-18] These two transitions are oriented roughly perpendicular to each other.[19] Low temperature steady state fluorescence polarization excitation spectra of tryptophan exhibit a structured excitation wavelength dependence.[20] This polarization behavior permits a decomposition of the absorption band into its two components. In polar solvents, the ^1L_a transition is believed to have a tail that extends to an energy lower than the limit of the ^1L_b transition. This suggests that essentially all of the observed emission comes from the ^1L_a state. The steady state anisotropy extracted from this type of analysis reaches a minimum value around 0.1 near 290 nm and a maximum value greater than 0.32 for excitation wavelengths greater than 300 nm.[20] The extensive overlap between these two transitions and the steady state fluorescence data indicate that the observed fluorescence anisotropy decay at short time will also be a strong function of excitation and emission wavelength.

A very important parameter in the evaluation of time-resolved fluorescence depolarization data is the experimental value of the anisotropy at zero time, $r(0)$. It is the intrinsic anisotropy of the chromophore and is a function only of the relative orientations of the absorption and emission transition dipole moments. For a chromophore with parallel absorption and emission transition dipoles the initial anisotropy is 0.4. Observations of experimental values of $r(0)$ less than the theoretically predicted value generally indicate the existence of relaxation processes occurring on a time scale shorter than the time resolution of the experiment. In steady state measurements, the extracted value of the initial anisotropy depends on the time integrated value of the anisotropy decay. Consequently, any fast decay components in the anisotropy are averaged out yielding $r(0)$ values less than the true limiting value. These processes can involve rotational or librational motion of the molecule,[15,21] or be due to purely electronic (vibronic) relaxation

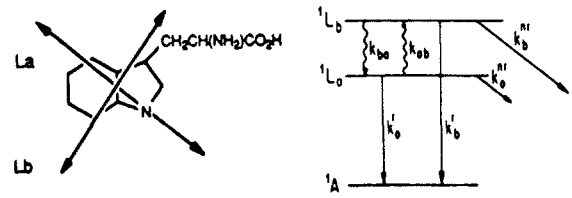

Figure 1. Two-level model for tryptophan excited state depolarization showing the relavent relaxation processes, the state ordering believed to exist in polar solvents, and the relative orientations of the transition dipole moments.

mechanisms.[22] Prior to this work, the theoretical limiting value [$r(0) = 0.4$] for tryptophan had never been observed. The origin of this low initial anisotropy has been of considerable concern because it severely complicates the interpretation of experimental data in terms of theory or molecular dynamics simulation. Converting a set of simulation coordinates to an anisotropy decay function, for example, requires a model for a low value of $r(0)$.[9] The nature of the assumptions made can significantly alter how the motion is reflected in the anisotropy decay. It is essential to know if an apparent reduction in the zero time anisotropy resulting from insufficient experimental time resolution indicates the existence of a rapid motional component that has been missed or is a manifestation of a non-motional electronic (vibronic) relaxation process. A knowledge of the relative time scales of electronic and motional contributions to the fluorescence depolarization is crucial since it determines the time range over which these processes can be cleanly separated.

Several possible explanations have been proposed over the years for the apparent reduction in the zero time anisotropy of tryptophan. These include exciplex formation,[23,24] fast torsional librations,[25] changes in the transition moment direction from the initially excited Franck-Condon state during solvation,[26,27] and the rapid interconversion of the ^1L_a and ^1L_b states.[28,29] In addition, it has been suggested that the emission band may actually be a superposition of unresolved vibronically induced transitions with alternate bands having orthogonal polarizations, thereby giving the appearance of a low average polarization.[30] All the explanations, except for the latter one, predict an initial fluorescence anisotropy of 0.4. Excitation into low-lying π,π^* configurations can lead only to in-plane polarized transitions. Consequently, the initial excitation creates a distribution of molecules with a preferred direction in the laboratory fixed coordinate system but does not distinguish in-plane orientations of the transition dipole of the two overlapping excited states. The relative time scales of the processes leading to the loss of memory of the initially excited distribution and the time resolution of the experiment determine the value of the initial anisotropy that is actually observed.

As pointed out by Cross et al.,[29] rapid depolarization of the emission can occur without the involvement of molecular motion. This was demonstrated with a simple two-state model for the fluorescence anisotropy decay of tryptophan that included the effects of ^1L_a,^1L_b level kinetics. The relevant relaxation processes involved in the kinetic scheme, the state ordering believed to exist in polar solvents, and the relationship of the transition dipole directions to the chromophore framework are shown in Figure 1. The expressions for the fluorescence anisotropy in this model

(6) Munro, R.; Pecht, I.; Stryer, L. *Proc. Natl. Acad. Sci., U.S.A.* **1979**, *76*, 56.
(7) Gratton, E.; Alacala, J. R.; Marriott, G. *Biochem. Soc. Trans.* **1986**, *14*, 835–838.
(8) McCammon, J. A.; Karplus, M. *Acc. Chem. Res.* **1983**, *16*, 187–193.
(9) Ichiye, T.; Karplus, M. *Biochemistry* **1983**, *22*, 2884–2893.
(10) MacKerrel, A. D., Jr.; Nilsson, L.; Rigler, R.; Saenger, W. *Biochemistry* **1988**, *27*, 4547–4556.
(11) McCammon, J. A.; Harvey, S. G. *Dynamics of Proteins and Nucleic Acids*; Cambridge University Press: Cambridge, 1987.
(12) Alber, T.; Kawasaki, G. *J. Mol. Appl. Genet.* **1982**, *1*, 419–434.
(13) Welch, G. R. *The Fluctuating Enzyme*; Wiley: New York, 1986.
(14) Chuang, T. J.; Eisenthal, K. B. *J. Chem. Phys.* **1972**, *57*, 5094–5097.
(15) Szabo, A. *J. Chem. Phys.* **1984**, *81*, 150–167.
(16) Mataga, N.; Torihasi, Y.; Ezumi, K. *Theor. Chim. Acta* **1964**, *2*, 158–167.
(17) Strickland, E. H.; Horwitz, J.; Billups, C. *Biochemistry* **1970**, *9*, 4914–4921.
(18) Strickland, E. H.; Billups, C.; Kay, E. *Biochemistry* **1972**, *11*, 3657–3662.
(19) Yamamoto, Y.; Tanaka, J. *Bull. Chem. Soc. Jpn.* **1972**, *45*, 1362–1366.
(20) Valeur, B.; Weber, G. *Photochem. Photobiol.* **1977**, *25*, 441–444.
(21) Zinsli, P. E. *Chem. Phys.* **1977**, *20*, 299–309.
(22) Hochstrasser, R. M. In *Probes of Biological Structure and Dynamics*, Proceedings of NATO Advanced Study Institute, Acireale, 1984; Szabo and Masotti, Eds.; p 165.
(23) Walker, M. S.; Bednar, T. W.; Lumry, R. *J. Chem. Phys.* **1967**, *47*, 1020.
(24) Walker, M. S.; Bednar, T. W.; Lumry, R.; Humphries, F. *Photochem. Photobiol.* **1971**, *14*, 147–161.
(25) Jablonski, A. *Acta Phys. Pol. B* **1965**, *28*, 717.
(26) Sun, M.; Song, P.-S. *Photochem. Photobiol.* **1977**, *25*, 3–9.
(27) Gonzalo, I.; Montoro, T. *J. Phys. Chem.* **1985**, *89*, 1608–1612.
(28) Andrews, L. J.; Forster, L. S. *Photochem. Photobiol.* **1974**, *19*, 353–360.
(29) Cross, A. J.; Waldeck, D. H.; Fleming, G. R. *J. Chem. Phys.* **1983**, *78*, 6455.
(30) Kalantar, A. H.; Albrecht, A. C. *Ber. Bunsenges. Phys. Chem.* **1964**, *68*, 361–376.

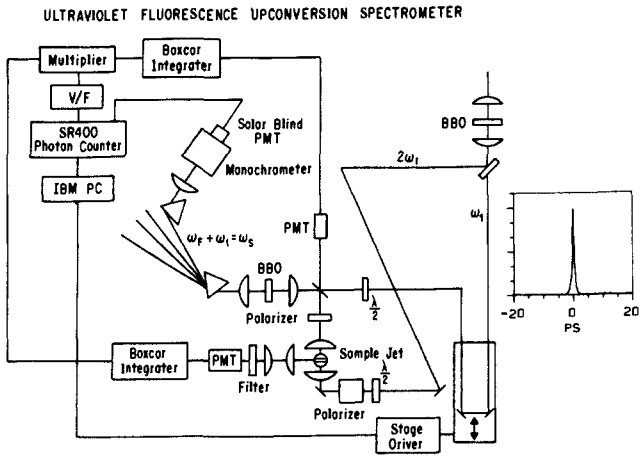

Figure 2. Schematic for the ultraviolet fluorescence upconversion spectrometer developed for this work. Inset: 500 fs cross correlation of the 578 nm dye laser fundamental with its second harmonic. Sum frequency detection at 192 nm. Legend: β-barium borate (BBO), photomultiplier (PMT), voltage to frequency converter (V/F), waveplate (λ/2).

contain orientational correlation functions involving the absorption and emission dipoles for the two states, $\mu^{(i)}_A$, $\mu^{(i)}_E$ with i = a,b, and the angle between the absorption dipole of one state and the emission dipole of the other state. This reversible two-state model predicts a biexponential form for both the anisotropy and population decays. The decay times and preexponential factors are complex functions of the kinetic constants of the system. The pre-exponential factors depend, in addition, on the ratio of ^1L_a to ^1L_b states initially prepared, the relative orientations of their absorption and emission transition dipoles, and their relative emission detection efficiencies. Given sufficient time resolution, the complex excitation and emission dependence of the fluorescence anisotropy predicted by this formulation of the depolarization problem provides a very useful experimental means of testing the two-level model of Figure 1.

In this work, we use frequency conversion optical gating to obtain an increase in time resolution of two orders of magnitude over previous measurements of fluorescence anisotropy of tryptophan. All our data can be interpreted with a generalized version of the model of Cross et al.[29] which also includes the effects of vibronic coupling.

Experimental Section

Excitation and gate pulses for the experiment were obtained from the amplified output of a modelocked cavity dumped dual jet hybrid R6G dye laser with chirp compensation. The dye laser was synchronously pumped with the second harmonic of a modelocked Spectron CW Nd:YAG laser. A combination of DODCI and DQOCI saturable absorber dyes was used in the absorber jet for wavelengths ≤590 nm; for wavelengths >590 nm a combination of DASBTI, DODCI, and DQOCI was used. Dye laser pulses with approximately 1.0 to 0.5 ps autocorrelation pulsewidths and 1 to 2 nm spectral bandwidths were cavity dumped and amplified at a 12 kHz repetition rate in a six pass sapphire jet amplifier[31] pumped by an Oxford copper vapor laser (CVL). No pulse broadening was observed after amplification. Synchronization between the CVL and the cavity dumped dye laser was achieved with a Camac Systems TS2000 timing system. In order to prevent long-term drift and timing errors associated with external triggering of the CVL thyratron, an optical feedback system was developed to maintain a fixed delay between the Camac timing pulses and the CVL optical pulses.

The ultraviolet fluorescence upconversion spectrometer developed for this work is shown in Figure 2. The second harmonic of the amplified dye laser pulse was generated by type I (o + o → e) mixing in β-barium borate (BBO). It was separated from the fundamental with a thin dichroic beamsplitter and used to excite the sample. The excitation polarization was selected with a Soliel-Babinet compensator and Glan-Thompson polarizer. The sample solution was flowed through a stainless steel dye jet nozzle to create a thin sample stream in air. During the course of the experiment the solution was continually degassed in the sample reservoir by bubbling with nitrogen. The sample temperature was maintained at 20 °C (measured just before the jet nozzle) with a temperature-regulated water bath and heat exchanger. No sample degradation was observed under the experimental conditions. Sample fluorescence was collected in a 180° geometry, passed through a polaroid HNP'B sheet polarizer, and recombined with the fundamental by reflection from a thin dichroic beamsplitter. The fluorescence and the dye laser fundamental were then focused into a second BBO crystal to generate the sum frequency by type I mixing. With the focusing conditions used in the experiment the upconversion bandwidth was approximately 4 nm. The emission detection frequency was selected by angle tuning the crystal to the appropriate phase-matching angle. The upconverted signal was isolated from the dye laser fundamental, second harmonic, and sample fluorescence with a pair of S1-UV quartz prisms, focused into an ISA Instruments HR320 monochrometer and detected by gated photon counting with a solar blind PMT.

The overall time resolution of the experiment is determined by the temporal widths of the excitation and gating pulses and the group velocity dispersion effects in the optics and mixing crystal. A 500 fs response function for the system generated by the cross-correlation of a 578 nm dye laser fundamental with its second harmonic and detected at 192 nm is shown in the inset on the left-hand side of Figure 2. The need for both spectral and temporal resolution in this experiment places a lower limit on the minimum usable laser pulsewidth. Both pulse width and pulse quality (lack of wings etc.) were used in determining the operating conditions at a given dye laser wavelength. Consequently the system response function varied between 500 fs and 1 ps depending on the experimental excitation wavelength.

Data acquisition and control of the optical delay line was achieved with an IBM PC/AT. Data was collected by repetitive scanning with ca. 1 s/pt integration times and either 100 fs/pt resolution for 20 ps scans or 1 ps/pt resolution for 200 ps scans. Individual scans within a given data set were later added together and analyzed by nonlinear least-squares fitting. Decay curves for fluorescence polarized parallel and perpendicular with respect to the excitation polarization were obtained on alternate scans of the delay line by rotating the polarization of the excitation pulse. Since the upconversion signal is proportional to the cube of the laser power, small changes in power can have a dramatic effect on the signal level. To ensure the integrity of the data, both the fluorescence intensity and the intensity of the dye laser fundamental were monitored and the count period was determined by their product. This procedure compensates for any laser power drifts and/or changes in sample fluorescence over the course of the data acquisition and thereby eliminates the need for tail matching of the parallel and perpendicular polarization anisotropy components. Accuracy of the fluorescence depolarization measurements was verified by the measurement of an initial anisotropy of 0.4 for stilbene in ethanol and comparison of the measured reorientational time (30 ps) with that obtained by anisotropic absorption (28 ps). L-Tryptophan was purchased from Sigma and used without further purification. The samples were prepared in pH 7 HPLC grade water at concentrations between 10^{-3} and 10^{-2} M. No concentration-dependent effects were observed.

Theory of the Measurement

The instantaneous power of the radiation generated at the sum frequency in a nonlinear optical mixing experiment is proportional to the product of the instantaneous power of the two input waves. In an optically sampled fluorescence measurement, a high power gate pulse is mixed with a low power fluorescence signal. For a fixed gate pulse power, the temporal shape of the fluorescence decay can be mapped out by delaying the gate pulse with respect to the fluorescence excitation pulse and measuring the upconverted power as a function of the optical delay. Since radiation at the sum frequency can only be generated when both waves are in the crystal simultaneously, the crystal acts as an optical sampling gate that is only open for the duration of the gate pulse. The observed signal at the sum frequency ($w_f + w$) as a function of delay time t', $S(t')$, is given by[32]

$$S(t') = \int_{-\infty}^{t'} I_{w_f}(t) P_w(t - t')\, dt \qquad (1)$$

where $P_w(t)$ is the pulse shape of the dye laser fundamental at frequency w, and $I_{w_f}(t)$ is the sample fluorescence intensity at time t and frequency w_f. The experimentally measured fluorescence intensity is related to the true fluorescence decay function, $i_{w_f}(t)$,

(31) Knox, W. H.; Downer, M. C.; Fork, R. L.; Shank, C. V. *Opt. Lett.* **1984**, *9*, 552–554.

(32) Beddard, G. S.; Doust, T.; Porter, G. *Chem. Phys.* **1981**, *61*, 17–23.

that would result with delta function excitation by the convolution operation

$$I_{wf}(t) = \int_{-\infty}^{t} i_{wf}(t')P_{2w}(t - t')\,dt' \quad (2)$$

where $P_{2w}(t)$ is the second harmonic excitation pulse shape. Combining eqs 1 and 2 gives

$$S(t') = \int_{-\infty}^{t'} i_{wf}(t)C_{3w}(t - t')\,dt \quad (3)$$

where $C_{3w}(t)$ is the measured cross-correlation function for the fundamental gate pulse and second harmonic excitation pulse given by

$$C_{3w}(t') = \int_{-\infty}^{t'} P_{2w}(t)P_w(t - t')\,dt \quad (4)$$

The cross correlation is measured by generation of the third harmonic of the dye laser in the same crystal and through the same optics used for upconversion of the sample fluorescence. It is the appropriate instrument response function for deconvolution of the optically gated fluorescence data and requires no assumptions about the laser pulse shape. In order to determine the fluorescence anisotropy decay, the sum frequency correlation functions for the polarization components of the emission polarized parallel, $I_{par}(t)$, and perpendicular, $I_{per}(t)$, to the excitation polarization are measured as well as the cross-correlation function for the gate and excitation pulses. The observed polarized emission curves are related to the impulse response decay functions, $i_{par}(t)$ and $i_{per}(t)$, by convolution with the cross-correlation function as shown previously. The excited state population decay law, $K(t)$, and the anisotropy decay law, $r(t)$, are related to the deconvoluted emission curves by[33]

$$i_{par}(t) = (1/3)K(t)[1 + 2r(t)] \quad (5)$$

$$i_{per}(t) = (1/3)K(t)[1 - r(t)] \quad (6)$$

Or equivalently

$$K(t) = i_{par}(t) + 2i_{per}(t) \quad (7)$$

$$r(t) = [i_{par}(t) - i_{per}(t)]/[i_{par}(t) + 2i_{per}(t)] \quad (8)$$

Data Analysis

The sum frequency anisotropy data were analyzed by simultaneous iterative reconvolution and nonlinear least-squares fitting of the parallel and perpendicular decay components as described by Cross and Fleming.[33] This method of simultaneous fitting acts directly on the raw data, taking into account the relationship that exists between parallel and perpendicular decay curves rather than on constructed anisotropy sum and difference functions. Fit quality was judged by the value of the χ^2 parameter and randomness of the modified residuals.[34,35] The Poisson counting statistics, on which these fitting procedures are based, are valid for time-correlated single-photon counting.[36] It is not clear that the same statistics should be valid for upconversion data obtained by gated photon counting and sequential data acquisition. Analysis of upconversion data using Poisson counting statistics, however, exhibits no unusual systematic errors and seems to satisfy the same statistical curve fitting criteria as time correlated single photon counting data. We therefore use the procedure described in ref 33 for fitting the upconversion data.

Anisotropy data sets (parallel and perpendicular polarization components) collected as a function of excitation and emission wavelength were first analyzed on an individual basis in order to examine the overall data surface. They were then reanalyzed using a global fitting procedure. Global analysis is a straightforward extension of the non-linear least-squares fitting procedure that allows several decay curves obtained under different experimental conditions to be fit simultaneously.[37-39] The multidimensional nature of the global technique can give better results than single curve fitting, because it exploits relationships that exist between different decay curves or in the case of anisotropy data, between different pairs of decay curves [$I_{par}(t)$ and $I_{per}(t)$], to overdetermine and constrain the model parameters.

The global approach offers two very important practical advantages in the analysis of data collected by frequency conversion optical gating. The complexity of optical gating experiments and the inherently low data accumulation rates usually associated with either laser repitition rate limitations and/or measurements on samples with small radiative rates makes the acquisition of individual decay curves with large numbers of total counts very difficult and time consuming. On the other hand, it is relatively easy to collect several decay curves in a reasonable amount of time by varying one of the experimental parameters, i.e. the emission detection wavelength, temperature, etc. This is significant, since the precision and accuracy of parameter estimation in global fitting is determined by the integral number of counts in the entire data surface. In addition, the global analysis procedure allows the dynamic range limitations associated with optical gating experiments to be overcome by allowing data sets obtained over long and short time ranges with different experimental time resolution to be mapped together. This permits a more accurate analysis of complex decays that have multiple decay components with very different time constants.

In agreement with the two-level kinetic model for tryptophan depolarization, the individual curve analysis of the tryptophan anisotropy data indicated that data collected over the entire excitation and emission data surface could in general be fit using a biexponential function for both $K(t)$ and $r(t)$

$$K(t) = \alpha_1 \exp(-t/\tau_1) + \alpha_2 \exp(-t/\tau_2) \quad (9)$$

$$r(t) = r_1 \exp(-t/\Phi_1) + r_2 \exp(-t/\Phi_2) \quad (10)$$

with a global linkage between the population lifetimes in each data set and depolarization lifetimes in each data set. Global analysis of the entire tryptophan excitation and emission data surface (12 anisotropy data sets) with this linkage scheme resulted in a good fit to the total decay surface (global $\chi^2 = 1.4$). Since the version of the global program used for this analysis did not fit a shift parameter between the data and response functions, these parameters were obtained from a single curve-fitting program that did have this ability. They were then input into the global program as fixed parameters. This results in slightly higher χ^2 values. The qualitative results of the analysis, i.e., general trends in the recovered parameters, however, were found to be insensitive to individual fit parameter values (values of fixed parameters, small changes in fitting range, shift parameter, etc.). Changes in these parameters resulted in only minor changes in the actual values of the recovered parameters. Globally linking only the population lifetimes or the depolarization lifetimes between data sets resulted in essentially the same recovered parameters as when both linkages were used simultaneously.

Since a negligible portion of the long-lifetime component (approximately 3.0 ns) in the total intensity decay is sampled over the 20 ps data collection range, this parameter is fixed at the weighted time averaged value calculated from the double exponential decay ($\alpha_1 = 0.22$, $\tau_1 = 0.6$ ns, $\alpha_2 = 0.78$, $\tau_2 = 3.2$ ns) determined for tryptophan in water by time-correlated single-photon counting.[40] The orientational correlation time for overall molecular tumbling was fixed at the value determined experimentally by fluorescence upconversion over a 200 ps time range.

Fluorescence Depolarization and Level Kinetics

Simulations of tryptophan time-resolved fluorescence anisotropy experiments including the effects of ^1L_a,^1L_b level kinetics were

(33) Cross, A. J.; Fleming, G. R. *Biophys. J.* **1984**, *46*, 45–56.
(34) Draper, N.; Smith, H. *Applied Regression Analysis*; John Wiley and Sons: New York, 1981.
(35) Bevington, P. R. *Data Reduction and Error Analysis for the Physical Sciences*; McGraw-Hill Inc.: New York, 1969.
(36) Grinwald, A.; Steinberg, I. Z. *Anal. Biochem.* **1974**, *59*, 583–598.
(37) Knutson, J. R.; Beechem, J. M.; Brand, L. *Chem. Phys. Lett.* **1983**, *102*, 501–507.
(38) Beechem, J. M.; Ameloot, M.; Brand, L. *Chem. Phys. Lett.* **1985**, *120*, 466–472.
(39) Beechem, J. M.; Ameloot, M.; Brand, L. *Anal. Instrum.* **1985**, *14*, 379–402.
(40) Petrich, J. W.; Chang, M. C.; McDonald, D. B.; Fleming, G. R. *J. Am. Chem. Soc.* **1983**, *105*, 3824–3832.

based on the treatment of fluorescence depolarization given by Cross et al.[29] A more general treatment by Szabo[15] gave identical results for this problem. In the algorithm of Cross et al., it is assumed that the excited-state dynamics can be described by first-order rate processes that are independent of the overall orientation of the molecules and that molecular reorientation occurs by anisotropic rotational diffusion. To simplify the problem, it is assumed that the rotational diffusion tensor is state independent. The excited-state populations are then given by

$$\frac{\mathrm{d}}{\mathrm{d}t} K^{(i)}(t) = \sum_{j=0}^{n-1} k_{ij} K^{(j)}(t) \qquad (11)$$

$$i = 0, 1, ..., n-1$$

where $K^{(i)}(t)$ is the number density of molecules in state (i), and k_{ij} is a matrix of first-order rate constants in the n-level system. The normalized orientational probability distribution for each level is defined such that the probability of finding a molecule in level (i) with an orientation between Ω and $\Omega + \mathrm{d}\Omega$ is proportional to $f^{(i)}(\Omega,t)\,\mathrm{d}\Omega$, and

$$K^{(i)}(t) = \int \mathrm{d}\Omega\, f^{(i)}(\Omega,t) \qquad (12)$$

where $\Omega \equiv (\alpha, \beta, \gamma)$, the Euler angles that specify the orientation of the molecular axis with respect to the laboratory fixed axis system, and the integration is over the limits $0 \le \alpha \le 2\pi$, $0 \le \beta \le \pi$, and $0 \le \gamma \le 2\pi$. Assuming that the orientation of the molecule does not change during a level-to-level transition, the set of coupled partial differential equations that describes the time evolution of the system can be written as[29]

$$\frac{\mathrm{d}}{\mathrm{d}t} f^{(i)}(\Omega,t) = -\sum_{\alpha=0}^{3} D_\alpha^{(i)} L_\alpha^2 f^{(i)}(\Omega,t) + \sum_{j=0}^{n-1} k_{ij} f^{(j)}(\Omega t) \qquad (13)$$

$$i = 0, 1, ..., n-1$$

where $D_\alpha^{(i)}$ ($\alpha = 1, 2, 3$) are the diagonal elements of the diffusion tensor in the molecular coordinate system for level (i), and L_α are the orbital angular momentum operators with respect to the molecular coordinate system as defined by Rose.[41] This set of equations can be solved by expanding the probability function for each level in terms of asymmetric rotor wave functions. The time evolution of the system can then be separated out and described in terms of the expansion coefficients. A detailed account of the methods used in solving this set of equations can be found in ref 29 and references therein. Since the absorption and emission transition dipoles are body fixed vectors in the molecular axis system, an effective excited-state emission anisotropy for each level can be defined with respect to an arbitrary absorption transition dipole, μ_A, such that

$$r^{(i)}(t) = [1/K^{(i)}(t)](^2/_5)^{1/2} 2\pi \sum_{T=-2}^{+2} a_{2T}^{(i)}(t)\, P_2(\mu^i_E \cdot \mu_A) \qquad (14)$$

where $P_2(x)$ is the second legendre polynomial, μ^i_E is the emission transition dipole for state i, and $a_{2T}^{(i)}(t)$ are expansion coefficients that describe the time evolution of the system. This formalism can be applied to the tryptophan energy level scheme in Figure 1 by defining the following parameters

$$k_a \equiv k_a^{\,r} + k_a^{\,nr} \qquad (15)$$

$$k_b \equiv k_b^{\,r} + k_b^{\,nr} \qquad (16)$$

$$\delta \equiv k_a + k_{ab} - k_b - k_{ba} \qquad (17)$$

$$Q \equiv [\delta^2 + 4k_{ab}k_{ba}]^{1/2} \qquad (18)$$

$$k \equiv k_a + k_{ab} + k_b + k_{ba} \qquad (19)$$

$$l_1 \equiv -{}^1/_2(k + Q) \qquad (20)$$

$$l_2 \equiv -{}^1/_2(k - Q) \qquad (21)$$

where the radiative and nonradiative rate constants for decay from the ^1L_a and ^1L_b states are given by k^r_a and k^r_b and k^{nr}_a and k^{nr}_b, respectively. The rate constants for interconversion between the two states are given by k_{ba} and k_{ab}. The excited-state populations obtained by solving eq 11 are then

$$K^{(a)}(t) = (1/2Q)\{K^{(a)}(0)[Q - \delta] + 2k_{ba}K^{(b)}(0)\} \exp(l_1 t) + (1/2Q)\{K^{(a)}(0)[Q + \delta] - 2k_{ba}K^{(b)}(0)\} \exp(l_2 t) \qquad (22)$$

and

$$K^{(b)}(t) = (1/2Q)\{K^{(b)}(0)[Q + \delta] + 2k_{ab}K^{(a)}(0)\} \exp(l_1 t) + (1/2Q)\{K^{(b)}(0)[Q - \delta] - 2k_{ab}K^{(a)}(0)\} \exp(l_2 t) \qquad (23)$$

Since the overall molecular tumbling behavior of tryptophan in water as measured by both fluorescence depolarization and anisotropic absorption[42] is well described by a monoexponential decay on the 35–45 ps time scale, it can be reasonably approximated as a spherical diffuser with a state-independent diffusion coefficient D over the time scale of interest in these initial simulations. This then leaves as parameters only the angles between the absorption and emission transition dipoles in each state. Setting $P_2(\mu^i_E \cdot \mu^j_A) = P_2(\cos\theta^{ij}_{EA})$ where θ^{ij}_{EA} is the angle between the emission transition dipole for state i and the absorption transition dipole of state j and defining angles θ^{aa}_{EA}, θ^{ab}_{EA}, θ^{bb}_{EA}, θ^{ba}_{EA} between the ^1L_a and ^1L_b absorption and emission transition dipoles μ^a_A, μ^b_A and μ^a_E, μ^b_E the anisotropy obtained for level a is then

$$r^{(a)}(t)K^{(a)}(t) = (2/5)(1/2Q)[\{K^{(a)}(0)P_2(\cos\theta^{aa}_{EA})[Q - \delta] + 2k_{ba}K^{(b)}(0)P_2(\cos\theta^{ab}_{EA})\} \exp[(l_1 - 6D)t] + \{K^{(a)}(0)P_2(\cos\theta^{aa}_{EA})[Q + \delta] - 2k_{ba}K^{(b)}(0)P_2(\cos\theta^{ab}_{EA})\} \exp[(l_2 - 6D)t]] \qquad (24)$$

and for level b

$$r^{(b)}(t)K^{(b)}(t) = (2/5)(1/2Q)[\{K^{(b)}(0)P_2(\cos\theta^{bb}_{EA})[Q + \delta] + 2k_{ab}K^{(a)}(0)P_2(\cos\theta^{ba}_{EA})\} \exp[(l_1 - 6D)t] + \{K^{(b)}(0)P_2(\cos\theta^{bb}_{EA})[Q - \delta] - 2k_{ab}K^{(a)}(0)P_2(\cos\theta^{ba}_{EA})\} \exp[(l_2 - 6D)t]] \qquad (25)$$

The total fluorescence anisotropy will then be given by

$$r(t) = [k_a^{\,r} g_a(w) r^{(a)}(t) K^{(a)}(t) + k_b^{\,r} g_b(w) r^{(b)}(t) K^{(b)}(t)] / [K^{(a)}(t) k_a^{\,r} g_a(w) + K^{(b)}(t) k_b^{\,r} g_b(w)] \qquad (26)$$

where $g_a(w)$ and $g_b(w)$ are spectral line shape functions. The intensities of the parallel and perpendicular components of the anisotropy are then

$$I_{par}(t) = (1/3)[k_a^{\,r} g_a(w) K^{(a)}(t)[1 + 2r^{(a)}(t)] + k_b^{\,r} g_b(w) K^{(b)}(t)[1 + 2r^{(b)}(t)]] \qquad (27)$$

and

$$I_{per}(t) = (1/3)[k_a^{\,r} g_a(w) K^{(a)}(t)[1 - r^{(a)}(t)] + k_b^{\,r} g_b(w) K^{(b)}(t)[1 - r^{(b)}(t)]] \qquad (28)$$

Radiative and nonradiative rate constants of 4.67×10^7 and 2.87×10^8 s^{-1}, respectively, were used to simulate tryptophan fluorescence depolarization experiments. These values were estimated by using an average lifetime for tryptophan of 3.0 ns, and assuming a quantum yield of 0.14. It was assumed that these constants apply to both the ^1L_a and ^1L_b states. The depolarization simulations are relatively insensitive to the actual values of these parameters since the dynamics on the picosecond time scale are dominated by the interconversion rate constants that are several orders of magnitude larger. The interconversion rate constants for the transitions between the two states k_{ba} and k_{ab} were obtained from the experimental upconversion data and the Boltzmann factor by assuming an ^1L_a,^1L_b level separation of 500 cm^{-1} at room temperature.

In the work of Cross et al., it was assumed that the absorption and emission transition dipoles that couple the ground state to

(41) Rose, M. E. *Elementary Theory of Angular Momentum*; Wiley: New York, 1957.

(42) Chen, L. X-Q.; Engh, R. A.; Fleming, G. R. *J. Phys. Chem.* **1988**, *92*, 4811–4816.

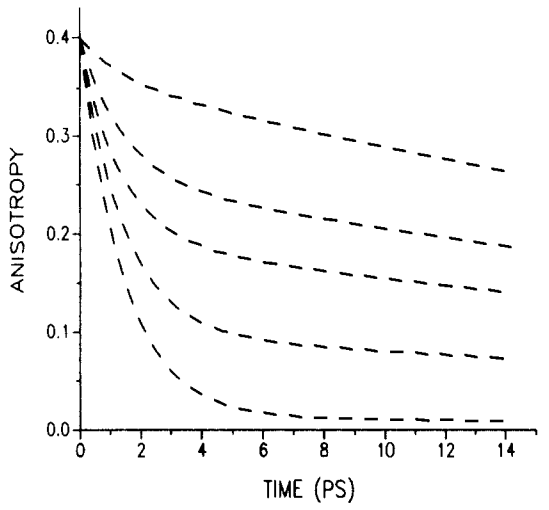

Figure 3. Simulations of fluorescence depolarization experiments for tryptophan with parameters described in the text and eqs 22, 23, 24, 25, and 26. Emission is detected with equal efficiency from both the ^1L_a and ^1L_b states. The angles between the transition dipoles are $\theta^{aa}{}_{EA} = 0$, $\theta^{ab}{}_{EA} = 90$, $\theta^{bb}{}_{EA} = 0$, $\theta^{ba}{}_{EA} = 90$. The ratios of initially excited states a:b are 1:0, 4:1, 2:1, 1:1, 1:2 (from top to bottom).

each excited state were parallel and the transition moments of the two excited states were perpendicular or at a large angle to each other ($\mu^{(a)}{}_A = \mu^{(a)}{}_E \neq \mu^{(b)}{}_A = \mu^{(b)}{}_E$). Anisotropy decays simulated with this depolarization model consist of a rapid decay corresponding to the attainment of a quasiequilibrium between the states and a slower decay corresponding to the overall rotational diffusion of the molecule. A corresponding fast decay component with a similar time constant is also present in the population decay. As shown in Figure 3 for $\theta^{aa}{}_{EA} = 0$, $\theta^{ab}{}_{EA} = 90$, $\theta^{bb}{}_{EA} = 0$, $\theta^{ba}{}_{EA} = 90$, i.e. for parallel absorption moments in each state and a 90° angle between the transition dipoles of the two states, the amplitude of these fast decay components decreases as the amount of preferential excitation or detection of the ^1L_a is increased. The decay rate, on the other hand, remains constant. The initial anisotropy of 0.4 and the biexponential form of the anisotropy decay is maintained for all excitation and emission detection conditions except those in which only a single state is initially excited and emission from only a single state is detected. In these cases, there is no fast decay component in the anisotropy and the level kinetics are reflected solely in the population decay. If the state that is initially excited is different than the state that is detected, the initial anisotropy will be lowered ($r(0) = -0.2$ for perpendicular transition moments) but no fast decay components or risetimes will appear in the anisotropy decay. It should be noted that this latter case is unrealistic for tryptophan in light of the extensive overlap of the ^1L_a and ^1L_b transitions.

If the absorption and emission moments in each state are no longer constrained to be parallel ($\mu^{(a)}{}_A \neq \mu^{(a)}{}_E \neq \mu^{(b)}{}_A \neq \mu^{(b)}{}_E$), the two-level model results in simulated anisotropy decays that can exhibit initial anisotropies varying from −0.2 to 0.4 with either decay times or risetimes in either or both the anisotropy and population decay. For a given set of kinetic constants and angles between transition dipoles, a series of curves with complex shapes can be generated that depend on the initial excitation condition and the detection efficiency of the two states. Examples of this type of depolarization behavior are shown in Figure 4, a–c. These sets of curves were generated by varying the initial excitation condition. The detection efficiencies were assumed to be equal for both states in Figure 4, a and b, and 60% ^1L_b detection in Figure 4c. In Figure 4a, the angle between the absorption and emission transition dipoles for the ^1L_a state is constrained to be parallel and all the other angles between transition dipoles are constrained to be perpendicular ($\theta^{aa}{}_{EA} = 0$, $\theta^{ab}{}_{EA} = \theta^{bb}{}_{EA} = \theta^{ba}{}_{EA} = 90$). This type of depolarization model results in anisotropy decays in which the initial anisotropy decreases as the amount of ^1L_b state initially excited or detected increases. Anisotropy decays simulated under these conditions all exhibit a fast decay

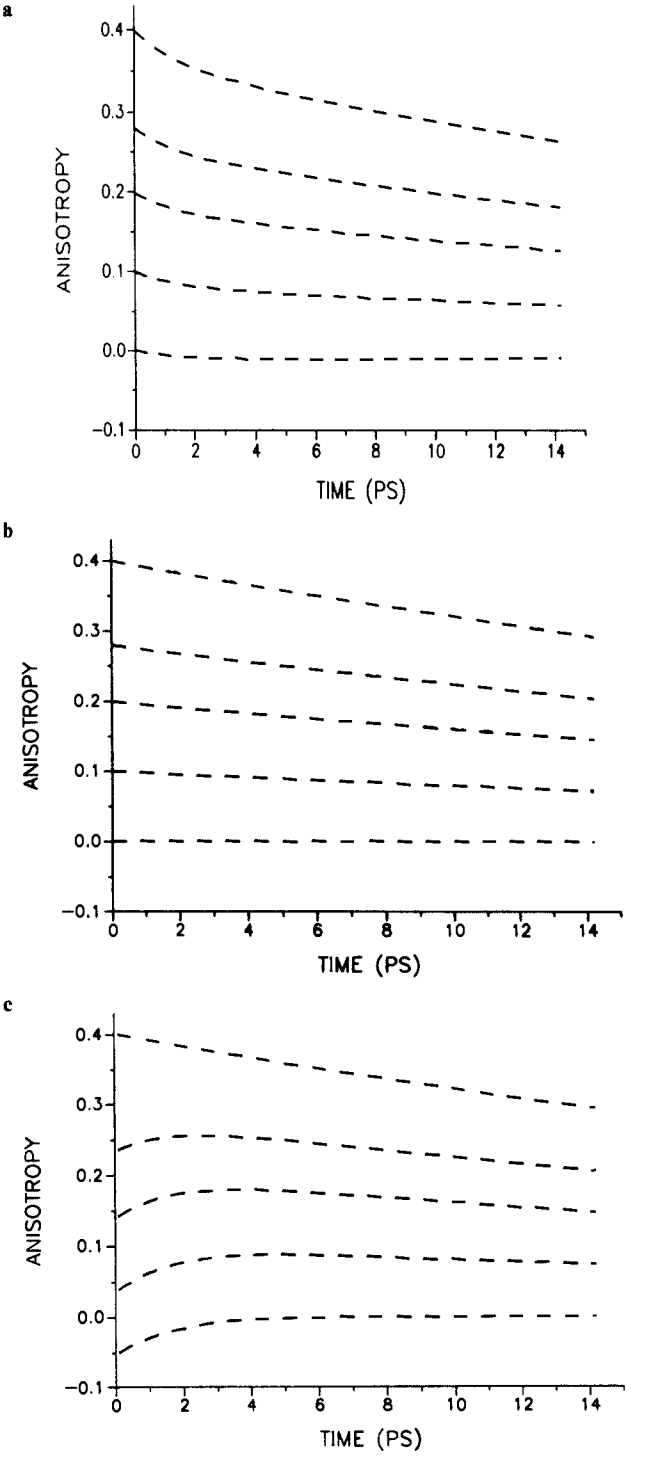

Figure 4. Simulations of fluorescence depolarization experiments for tryptophan with parameters described in the text and eqs 22, 23, 24, 25, and 26. Emission is detected with equal efficiency from both the ^1L_a and ^1L_b states in (a) and (b) and with 60% ^1L_b efficiency in (c). The ratios of initially excited states a:b are 1:0, 4:1, 2:1, 1:1, 1:2 (from top to bottom). (a) The angles between the transition dipoles are $\theta^{aa}{}_{EA} = 0$, $\theta^{ab}{}_{EA} = \theta^{bb}{}_{EA} = \theta^{ba}{}_{EA} = 90$. (b) The angles between the transition dipoles are $\theta^{aa}{}_{EA} = 0$, $\theta^{ab}{}_{EA} = 90$, $\theta^{bb}{}_{EA} = 90$, $\theta^{ba}{}_{EA} = 0$. (c) The angles between the transition dipoles are $\theta^{aa}{}_{EA} = 0$, $\theta^{ab}{}_{EA} = 90$, $\theta^{bb}{}_{EA} = 90$, $\theta^{ba}{}_{EA} = 0$.

component in both the anisotropy and population decay with an excitation- and emission-dependent amplitude. Setting the angle between the absorption dipole of the ^1L_a state and the emission dipole of the ^1L_b state equal to zero ($\theta^{aa}{}_{EA} = 0$, $\theta^{ab}{}_{EA} = 90$, $\theta^{bb}{}_{EA} = 90$, $\theta^{ba}{}_{EA} = 0$) results in the anisotropy decays shown in Figure 4b. In this case, the initial anisotropy decreases with increasing ^1L_b excitation and/or detection, but there is no fast decay component in the anisotropy. A fast decay component with the excitation and emission characteristics mentioned earlier does

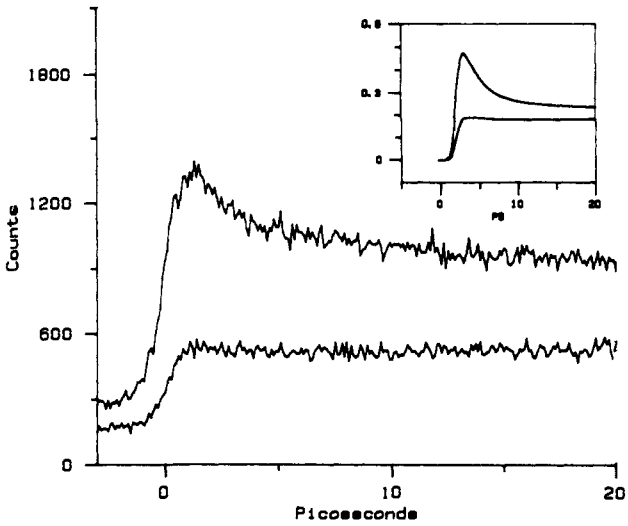

Figure 5. Parallel (top curve) and perpendicular polarization components of the tryptophan emission (300 nm excitation, 330 ± 5 nm fluorescence, 600 nm gate pulse, upconverted signal detected at 213 nm). Inset: Simulated data. See text.

however exist in the population decay. The anisotropy decreases from its initial value over the 15 ps time scale of the simulation for initial conditions involving <50% ^1L_b excitation and increases from its initial value when >50% of this state is excited. Using the same transition dipole orientations and increasing the ^1L_b detection ratio to 60% results in the curves shown in Figure 4c. This model also results in initial anisotropies that decrease with increasing ^1L_b excitation but exhibit risetimes in the anisotropy. Depending on the initial excitation and emission detection conditions there can be either risetimes or decay times in the population decay. Of course, the examples in Figure 4 represent limiting cases of the type of depolarization behavior that might be observed. Angles between transition dipoles other than 0° and 90° result in less dramatic effects of the same type.

Physically, different angles between transition moments in the two-level model can be interpreted in terms of the interactions between close-lying vibronically coupled states. Within this framework, each vibronic transition of tryptophan is associated with a specific absorption and emission transition dipole resulting from the vibronic mixing of ^1L_a and ^1L_b states. A time scale separation is assumed to exist between internal conversion and vibrational relaxation, so that transitions between different vibronic levels within the two excited-state manifolds can be thought of as instantaneous rotations of the absorption and emission transition dipoles. The angles between transition moments in the two-level model then reflect the differences in transition dipole orientation between the initially excited Frank–Condon vibronic states and the vibronic levels that are detected in emission. Short time dynamics result from the interconversion between ^1L_a and ^1L_b states while the initial anisotropy and actual shapes of the decays are determined by the angular differences in transition moments between vibronic states resulting from vibronic coupling.

Results and Discussion

Many of the qualitative features of the tryptophan anisotropy data that are essential to our discussion of tryptophan fluorescence depolarization are directly observable in the raw experimental data. Consequently, the conclusions that are drawn are not dependent on the numerical data analysis procedures. The detailed data analysis in most cases simply permits a quantitative presentation of the results. For example, the raw parallel and perpendicular polarization decay components for tryptophan in water excited at 300 nm are shown in Figure 5. The anisotropy constructed from these decays is shown along with the global nonlinear least-squares fit to the data in Figure 6. Fluorescence at 330 nm (±5 nm) on the short wavelength edge of the steady-state tryptophan emission spectrum was mixed with the 600-nm fundamental to produce the upconverted signal near 213 nm. A rapid

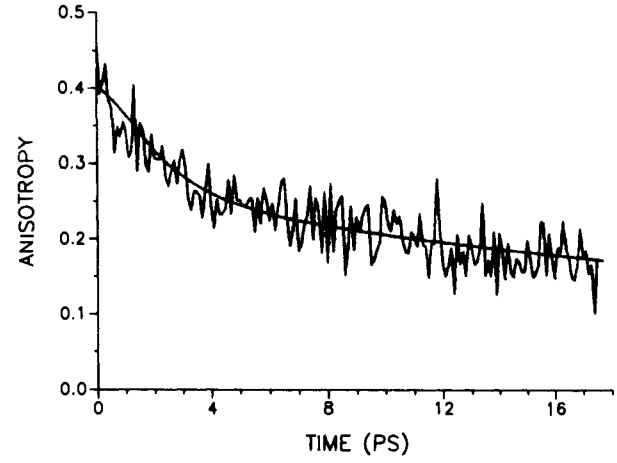

Figure 6. Anisotropy decay constructed from the polarization decay components in Figure 5 (300 nm excitation, 330 ± 5 nm fluorescence). The solid line is the global nonlinear least-squares fit to the data.

picosecond decay component can be seen in the parallel polarization component of the emission. The raw anisotropy data have an initial anisotropy of 0.4 and a similiar fast decay component along with the much longer component due to the overall tumbling of the molecule. A short decay component is also found on this time scale in the total intensity decay of the fluorescence. Data simulated with use of the two-level model for fluorescence depolarization are shown in the inset of Figure 5. The parameters used in these simulations were chosen to approximate the experimental conditions, i.e. long wavelength mostly ^1L_a excitation and detection of short wavelength mostly ^1L_b emission. Use of an initial condition involving ^1L_b excitation at this relatively long wavelength is supported by the recent two-photon steady-state polarization data of Callis et al.[43] for tryptophan in water. These data indicate that at least 7% ± 5% of the absorption at 300 nm is due to the ^1L_b state. It is interesting to note that the relatively simple two-level model for fluorescence depolarization qualitatively reproduces the experimentally observed shapes of both polarization components. The shape of the perpendicular emission component is quite unusual. For purely orientational motion one would expect this polarization component to exhibit a simple risetime correlated with the decay of the parallel polarization component. The squared off shape of the curve and the small dip in the data at about 2 ps results from the existence of a decay component in the population decay that is much shorter than the overall molecular reorientation time. The belief that ^1L_b emission is being detected in these experiments is supported by the emission and excitation wavelength behavior of the short decay component amplitude in the total intensity decay as shown in Figure 7, a and b. Increasing either the excitation wavelength or emission detection wavelength decreases the amplitude of this component as expected. Agreement between the data and the simulations is also not possible without assuming that fluorescence from the ^1L_b state is present. Although dual ^1L_a, ^1L_b emission has been implicated in previous photophysical studies of tryptophan,[44,45] this is the first direct experimental evidence for its existence based on time-resolved fluorescence data.

Examination of the raw parallel polarization components of the anisotropy data as a function of excitation and emission wavelength provides a useful overview of the tryptophan depolarization data. Activity in both the population decay and anisotropy decay is reflected in these curves. The parallel polarization components for anisotropy data collected with 300 nm excitation as a function of emission detection wavelength (330, 335, 340, 360, and 380 nm) are shown in Figure 8. The parallel polarization

(43) Callis, P. R.; Rehms, A. A. Private communication.
(44) Chernitskii, E. A.; Konev, S. V. *Dokl. Akad. Nauk Belorussk SSR* **1964**, *8*, 258.
(45) Konev, S. V.; Bobrovich, V. P.; Chernitskii, E. A. *Dokl. Akad. Nauk SSSR* **1965**, *10*, 341–345.

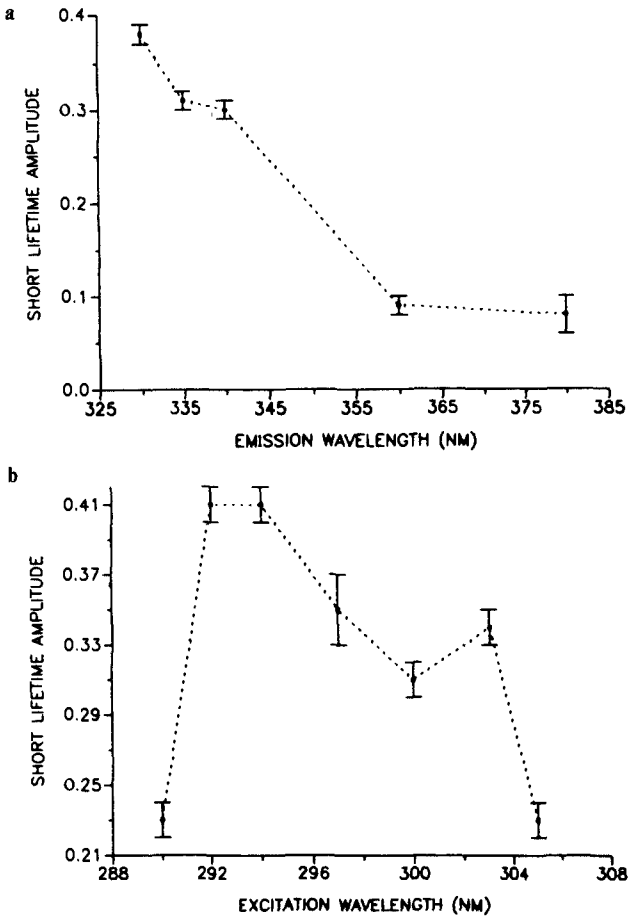

Figure 7. (a) Emission dependence of the short decay component amplitude in the tryptophan total intensity decay. (b) Excitation dependence of the short decay component amplitude in the tryptophan total intensity decay. Dashed lines are meant only to guide the eye.

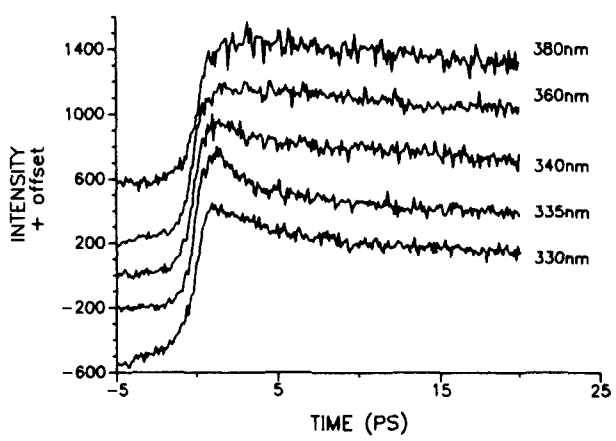

Figure 8. Emission dependence of the parallel polarization components of the tryptophan anisotropy data. The raw data have been normalized, multiplied by the initial anisotropy and offset for clarity. Excitation at 300 ± 1 nm.

components from the data collected as a function of excitation wavelength (289, 290, 292, 294, 297, 300, 303, 305 nm) at the same short wavelength edge of the steady-state emission band (330 nm) are shown in Figure 9. In accord with the qualitative predictions of the two-level model, increasing the excitation and/or emission detection wavelength, i.e. increasing the ratio of $^1L_a/^1L_b$ initially excited or detected, results in a decrease in the amplitude of the short time components in these decays. An interesting comparison of these data can also be made with anisotropy data collected under identical experimental conditions, with long wavelength excitation (303 nm) and short wavelength emission detection (335 nm) for 5-methoxytryptophan (top curve in Figure

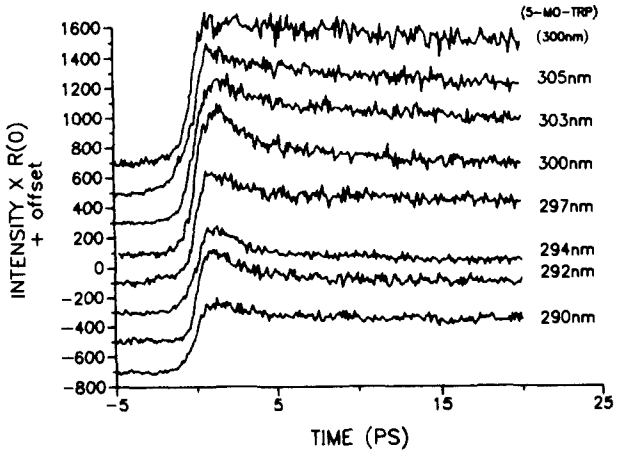

Figure 9. Excitation dependence of the parallel polarization components of the tryptophan anisotropy data. Fluorescence at 335 ± 5 nm was detected. The raw data have been normalized and multiplied by the initial anisotropy determined from global analysis of the data.

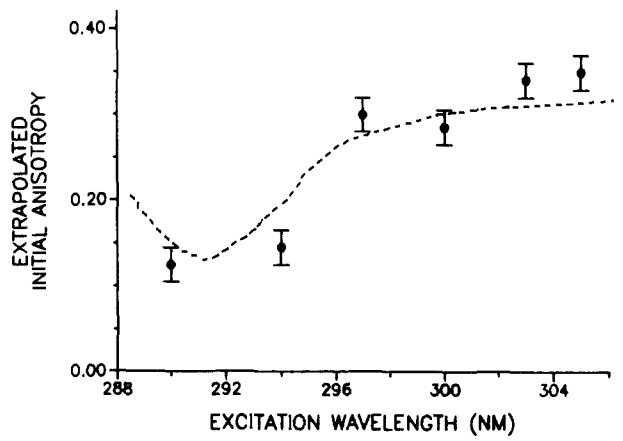

Figure 10. Excitation dependence of the initial anisotropies obtained by extrapolation back to $t = 0$ from the long time anisotropy decay component (330 ± 5 nm fluorescence detection, excitation wavelength ± 1 nm). The dashed line is the digitized low-temperature static fluorescence polarization excitation data of Valeur and Weber.[20]

9). This molecule is known to have its ^1L_b state at lower energy than the ^1L_a state and to have a much greater ^1L_a, ^1L_b level separation than tryptophan.[18,46,47] In agreement with the model, 5-methoxytryptophan exhibits an initial anisotropy of 0.4, with a fast decay component in the anisotropy with negligible amplitude. The most notable feature of the raw tryptophan anisotropies constructed at these excitation wavelengths is that the initial anisotropy exhibits an excitation dependence that monotonically decreases from an $r(0) = 0.4$ at wavelengths ≥300 nm to an $r(0) = 0.14$ at 290 nm. As shown in Figure 10, the values of $r(0)$ at these excitation wavelengths obtained by extrapolation back to $t = 0$ from the long time decay component are in good agreement with the low-temperature static fluorescence polarization excitation data of Valeur and Weber,[20] indicating that the data are internally consistent.

For comparison with the data of Figure 6 that were collected on the short wavelength edge of the tryptophan emission spectrum, an example of a raw anisotropy decay collected with 300-nm excitation and detected at 380 nm along with the fit to the data is shown in Figure 11. It is important to remember that the shapes of the decays that are experimentally observed depend on both the initial excitation condition and the detection efficiency of the two states. In other words, if both states were initially excited, but the experimental time resolution was not sufficient to detect

(46) Lami, H.; Glasser, N. J. Chem. Phys. 1986, 84, 597-604.
(47) Gudgin-Templeton, E. F.; Ware, W. R. Chem. Phys. Lett. 1983, 101, 345-349.

Table I. Global Analysis Results for Tryptophan/Water (pH 7, 20 °C) Anisotropy Data[a]

Ex (±1 nm)	Em (±5 nm)	$r(0)$	r_1	r_2	α_1	α_2
305	335	0.40 ± 0.02	0.07 ± 0.01	0.33 ± 0.01	0.23 ± 0.01	0.77 ± 0.01
303	335	0.42 ± 0.02	0.09 ± 0.01	0.33 ± 0.01	0.34 ± 0.01	0.66 ± 0.01
	340	0.39 ± 0.02	−0.02 ± 0.01	0.41 ± 0.01	0.28 ± 0.01	0.72 ± 0.01
300	330	0.40 ± 0.02	0.05 ± 0.01	0.35 ± 0.01	0.38 ± 0.01	0.62 ± 0.01
	335	0.42 ± 0.02	0.17 ± 0.01	0.35 ± 0.01	0.31 ± 0.01	0.69 ± 0.01
	340	0.39 ± 0.02	−0.02 ± 0.01	0.41 ± 0.01	0.30 ± 0.01	0.70 ± 0.01
	360	0.39 ± 0.02	−0.04 ± 0.01	0.43 ± 0.01	0.09 ± 0.01	0.91 ± 0.01
	380	0.39 ± 0.02	−0.05 ± 0.02	0.44 ± 0.01	0.08 ± 0.02	0.92 ± 0.01
297	335	0.30 ± 0.02	−0.03 ± 0.02	0.33 ± 0.01	0.35 ± 0.02	0.65 ± 0.01
297	340	0.30 ± 0.02	−0.04 ± 0.02	0.34 ± 0.01	0.39 ± 0.02	0.61 ± 0.01
294	335	0.26 ± 0.02	0.15 ± 0.01	0.11 ± 0.01	0.41 ± 0.01	0.59 ± 0.01
292	335	0.25 ± 0.02	0.01 ± 0.01	0.24 ± 0.01	0.41 ± 0.01	0.59 ± 0.01
290	335	0.17 ± 0.02	0.07 ± 0.01	0.10 ± 0.01	0.23 ± 0.01	0.77 ± 0.01

[a] $r(t) = r_1 \exp(-t/\Phi_1) + r_2 \exp(-t/\Phi_2)$; $\Phi_1 = 2.0 \pm 0.2$ ps, $\Phi_2 = 45$ ps; $r(0) = r_1 + r_2$; $K(t) = \alpha_1 \exp(-t/\tau_1) + \alpha_2 \exp(-t/\tau_2)$; $\tau_1 = 1.6 \pm 0.2$ ps, $\tau_2 = 1692$ ps; $1 = \alpha_1 + \alpha_2$.

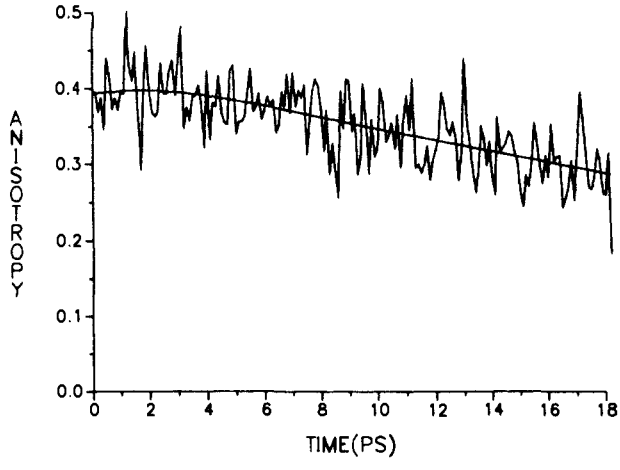

Figure 11. Tryptophan anisotropy decay collected with 300 ± 1 nm excitation and detecting fluorescence at 380 ± 5 nm. The solid line is the global nonlinear least-squares fit to the data.

emission from the ^1L_b state, the resulting anisotropy would exhibit not only a low initial anisotropy but also a differently shaped decay curve at short time. The type of curvature in Figure 11, for instance, would not be detected.

A more detailed comparison with the two-level depolarization model can be made by examining the parameters recovered from the deconvolution and nonlinear least-squares fitting of the data. The recovered parameters from the global analysis of the excitation/emission data surface are shown in Table I. The longer decay components in the anisotropy and total intensity decay were fixed at 45 and 1692 ps as discussed earlier with regard to data analysis. It should be noted that the ability to successfully analyze the anisotropy data with a biexponential model that incorporates global linkages between the short time decay components in the anisotropy and total intensity decay in itself lends support to the two-level model for the fluorescence depolarization of tryptophan. The global linkage scheme discussed earlier resulted in a 1.6 ± 0.2 ps component in the total intensity decay. The short time decay component in the anisotropy decay was determined by global analysis to be 2.0 ± 0.2 ps. Single curve analysis resulted in values for both these parameters scattered between 1.0 and 4.0 ps. The excitation and emission dependence of the short lifetime component amplitude in the population decay are shown in Figure 7, a and b. Although the time constants obtained from biexponential fits to the data are in general complex combinations of the kinetic constants that parametrize the two-level model, the time scale separations in this problem mean that the 1.6-ps component essentially represents the ^1L_b to ^1L_a internal conversion rate.

The excitation and emission dependence of the short time anisotropy decay component amplitude are shown in Figure 12, a and b. A striking observation in Figure 12a is the large decrease in decay amplitude at 297 and 292 nm. These are reproducible features of the anisotropy decay surface. It is interesting to note that the absorption in indole and its derivatives at 297 nm has

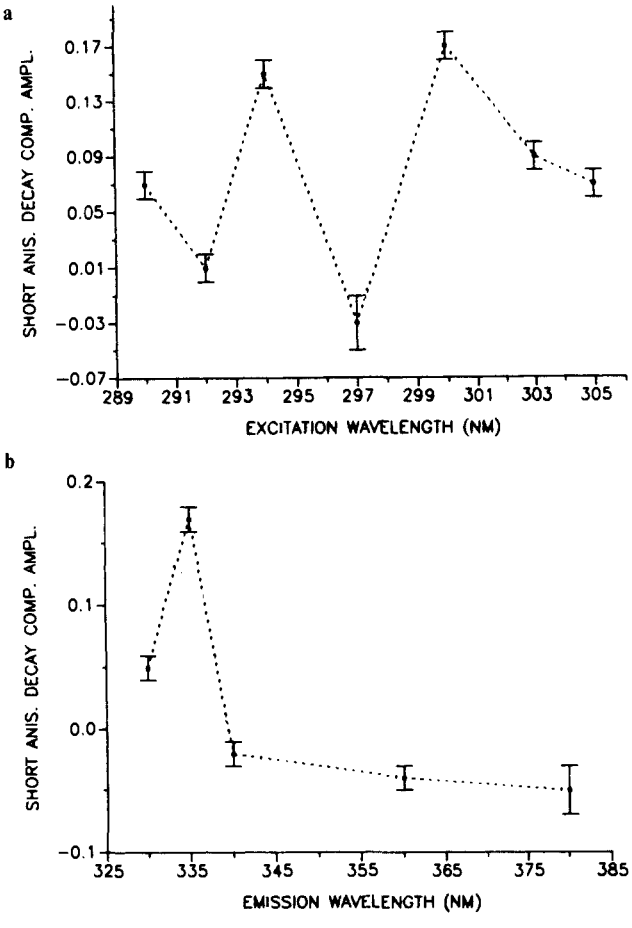

Figure 12. (a) Excitation dependence of the short time anisotropy decay component amplitude. (b) Emission dependence of the short time anisotropy decay component amplitude. Dashed lines are meant only to guide the eye.

been assigned to the 0–760 cm^{-1} hot band for the ^1L_b transition.[17] One can speculate that the 292 nm excitation may involve a hot band as well. The rapid decrease in the short time anisotropy decay amplitude with emission wavelength, between 335 and 340 nm, while unusual may simply represent the peculiarities of the relative dipole moment orientations of the vibronic transitions involved in the absorption and emission process as discussed below. The excitation dependence of the initial anisotropy extracted from fits to the data is shown in Figure 13.

The convoluted anisotropy decays calculated from the fit parameters as a function of excitation and emission wavelength are shown in Figures 14a and 15a. Anisotropy decays (impulse response) simulated with the two-level model are shown in Figures 14b and 15b. The parameters used in the tryptophan depolarization simulations are given in Table II. By using values for the $^1L_b/^1L_a$ excitation ratio consistent with those determined by Callis

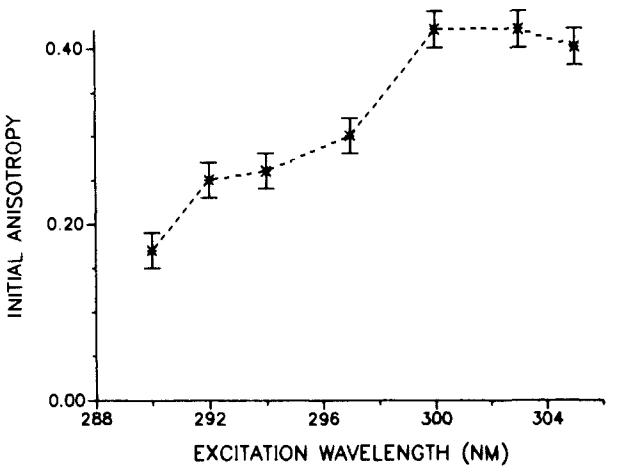

Figure 13. Excitation dependence of the initial anisotropy determined from global analysis of the data. Dashed lines are meant only to guide the eye.

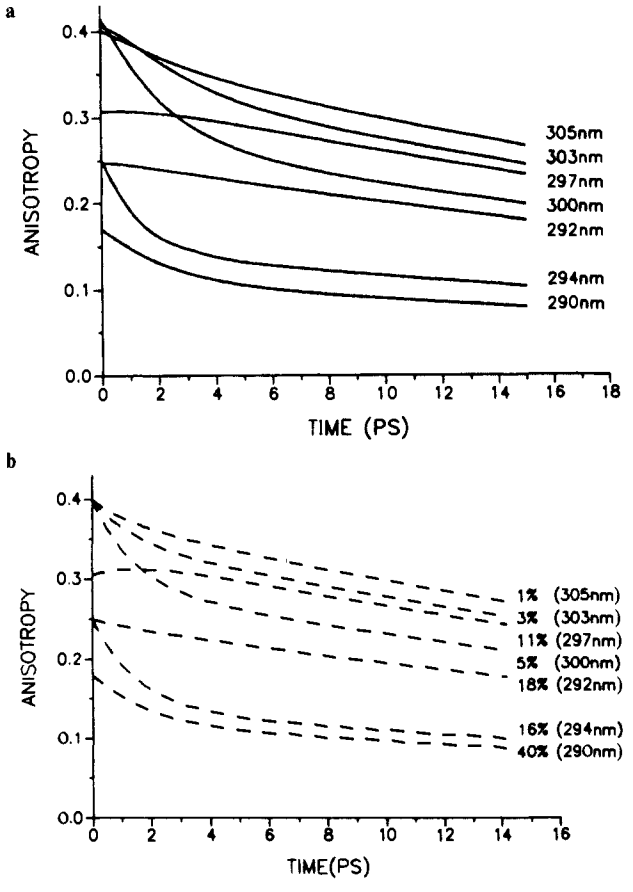

Figure 14. (a) Convoluted anisotropy decays obtained from biexponential global fits to the depolarization data collected with 305, 303, 300, 297, 294, 292, and 290 nm excitation, and an emission detection wavelength of 335 ± 5 nm. (b) Simulations of tryptophan anisotropy decay data shown in Figure 14a with use of the depolarization model and parameters discussed in the text. The $^1L_b/^1L_a$ excitation ratio at a given experimental excitation wavelength was chosen to be in agreement with the two-photon fluorescence depolarization results of Callis et al.[42] The $^1L_b/^1L_a$ detection efficiency was assumed to be 65 ± 5%. The angles assumed between the transition dipoles are given in Table II.

et al.[43] and reasonable estimates of the experimental detection efficiency for the two states, the two-level model can qualitatively reproduce the experimentally observed features in the tryptophan anisotropy decays as a function of excitation and emission wavelength. To obtain agreement with the fits to the experimental data, it is necessary to assume that both ^1L_a and ^1L_b states are excited and emission from both states is detected. In particular, in order to duplicate the wavelength dependence of $r(0)$, the lack

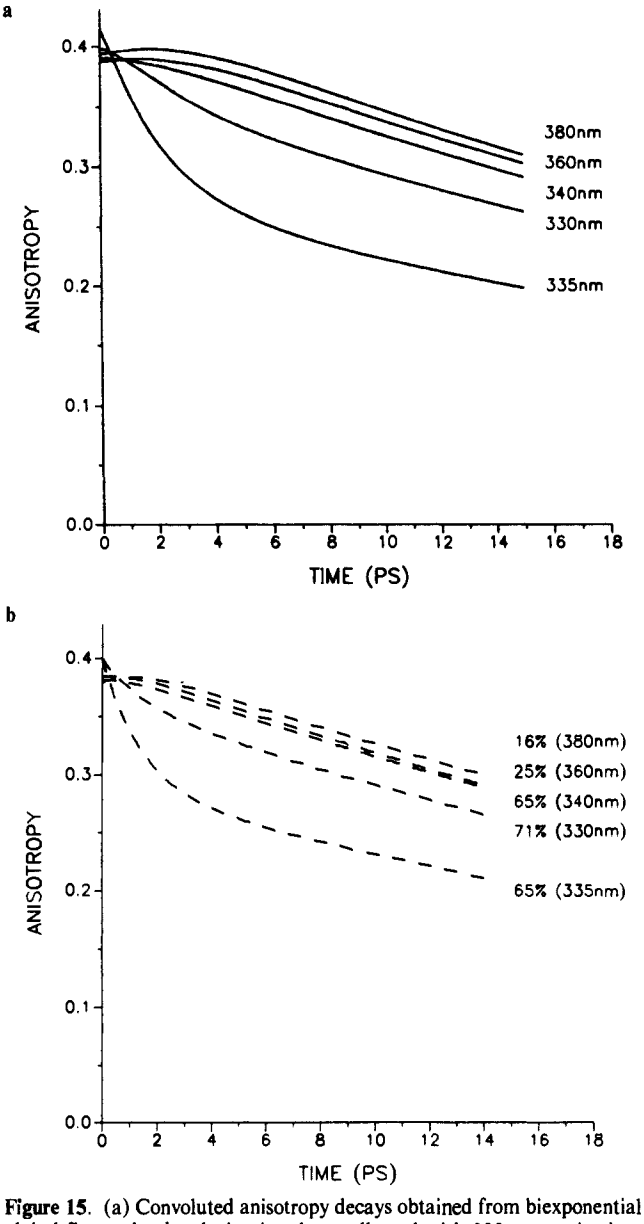

Figure 15. (a) Convoluted anisotropy decays obtained from biexponential global fits to the depolarization data collected with 300-nm excitation, at emission detection wavelengths of 330 ± 5, 335 ± 5, 340 ± 5, 360 ± 5, and 380 ± 5 nm. (b) Simulations of tryptophan anisotropy decay data shown in Figure 15a with use of the depolarization model and parameters discussed in the text. An $^1L_b/^1L_a$ excitation ratio of 5% was assumed. The $^1L_b/^1L_a$ detection efficiency was varied from 70% to 10%. The angles assumed between the transition dipoles are given in Table II.

of short decay components at specific wavelengths, and the unusual forms of the anisotropy curves, it is necessary to allow the angle between the absorption and emission moments of the two states to vary with both excitation and emission wavelength. Ultrafast vibrational relaxation from Franck–Condon states to relaxed levels with rotated transition moments and vibronic coupling effects in the emission spectrum are plausible suggestions for these two non-motional mechanisms for lowered anisotropy. Because of the large number of correlated parameters no attempt was initially made to fit the raw experimental data directly with the model or extract a unique spectral dependence of the transition moment orientations. The values in Table II were chosen to demonstrate the feasibility of the two-level model, and they simply represent one possible combination of parameters that qualitatively reproduce the data. An exhaustive search of parameter space was not made. Some of the transition dipole orientations used in the simulations involve out-of-plane emission intensity. This may not be unreasonable for a low-symmetry molecule like tryptophan in a strongly associating solvent like water. In addition, it should be noted that in order to reproduce the shapes of the 360 and 380

Table II. Parameters Used in Tryptophan Depolarization Simulations[a]

simulated Ex (nm)	experiment Em (nm)	excitation ratio (%) $^1L_b/(^1L_a + ^1L_b)$	emission detection efficiency (%) $^1L_b/(^1L_a + ^1L_b)$	θ_{EA}^{aa}	θ_{EA}^{bb}	θ_{EA}^{ba}	θ_{EA}^{ab}
305	335	1	65	0	0	40	40
303	335	3	65	0	0	50	50
300	330	5	71	0	0	30	30
	335	5	65	0	0	90	90
	340	5	65	0	30	0	30
	360	5	25	5	90	0	0
	380	5	16	10	90	0	0
297	335	11	65	0	90	0	90
294	335	16	65	30	30	90	90
292	335	18	65	0	90	90	90
290	335	40	65	0	50	90	90

[a] $k_{ba} = 0.625$ ps^{-1}; $k_{ab} = 0.044$ ps^{-1}; $k_{ar} = k_{br} = 4.67 \times 10^{-5}$ ps^{-1}; $k_{anr} = k_{bnr} = 2.87 \times 10^{-4}$ ps^{-1}; $1/6D_{rot} = 45$ ps.

nm anisotropy data either large ^1L_b detection efficiencies or angles inconsistent with the original definition of the transition dipole orientations appeared to be necessary. These complications in modeling the depolarization dynamics on the long-wavelength edge of the ^1L_b emission may be a manifestation of the differential solvation dynamics of the ^1L_a and ^1L_b states after their interconversion. In other words, the dynamic stokes shift associated with the changing excited state dipole moments is modulated by the interconversion kinetics. Despite these difficulties, the overall agreement with the model is very good. The main point is that although the values in Table II may not be unique, they serve to illustrate the fact that by allowing the ^1L_a and ^1L_b transition moments to vary significantly over the absorption and emission surface the simple two-level model can qualitatively describe the main features of the anisotropy data.

The discussion given above suggests that the initial schematic describing the two-state model in Figure 1 should be replaced with the more complex model in Figure 16 that includes vibronic levels in addition to the ^1L_a and ^1L_b states. If the ^1L_a and ^1L_b states are vibronically coupled as might be expected for two close-lying excited states, the transition dipole moment connecting the various vibronic states will be frequency dependent.[48-50] The initially excited vibronically mixed state may have a different dipole moment direction than the vibrationally relaxed fluorescence state. Consequently, if the excitation is high in the vibrational manifold, emission from the initially photoselected distribution of molecules will depolarize with a rate corresponding to that for vibrational relaxation. The amplitude of the decay will be determined by the amount of vibronically mixed character in the initial and final states and therefore on the initial excitation condition.

The same type of argument can be applied to probing the emission spectra after excitation into the region near the zero vibrational level of the excited states. In this case, the polarization of the vibronic transition in fluorescence can depend on the displacement along the vibrational mode mixing the two electronic states that are coupled.[51-53] Consequently, the amount of vibronically mixed character and the relative transition dipole orientations can vary across the emission band. The situation in tryptophan is especially complicated since its low molecular symmetry makes it a multimode problem. In our experiments, we are detecting both long-wavelength ^1L_b emission as well as short-wavelength ^1L_a emission. Depending on the excitation wavelength these are often hot band transitions. It is reasonable to assume that the orientations for the absorption and emission transition dipoles may be different.

The vibronic energies of the states and the strength of their coupling can depend significantly on local solvation structures and the molecular motions of the solvent on the femtosecond time scale (<500 fs). Solvation dynamics[54,55] would severely complicate the analysis of fluorescence depolarization on this time scale since both the rate constants and transition dipole orientations would be time dependent. Fluorescence anisotropy data on the subpicosecond time scale (>500 fs) on the other hand appear to be dominated by the effects of internal conversion between the ^1L_a and ^1L_b states. Vibronic coupling and solvation effects result in essentially instantaneous rotations of the transition dipoles and are reflected in the values of the angles between transition moments in the two-level model. It is the time scale separation between these different depolarization mechanisms that allows this simple model to describe the tryptophan depolarization data.

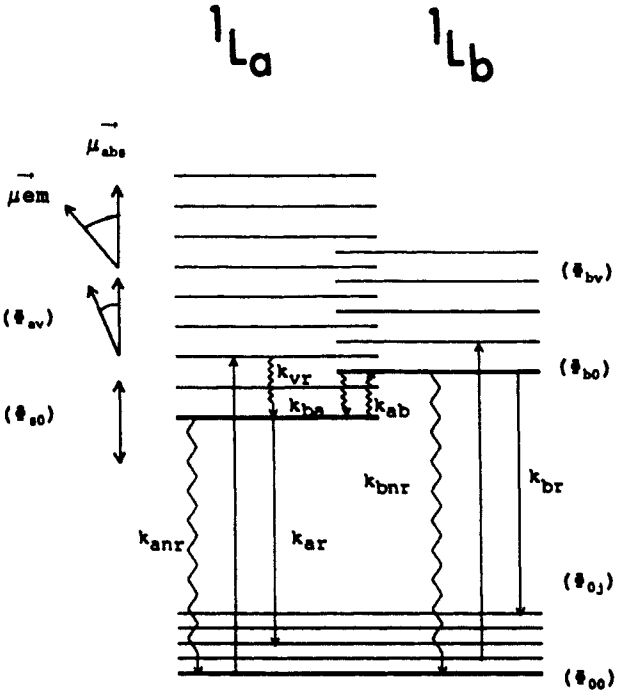

Figure 16. Generalized two-level model for tryptophan depolarization. Each vibronic level, Φ_{0j}, in the ground state and excited states, Φ_{iv} with i = a, b, is associated with specific absorption, and emission transition dipoles (μ_{abs}, μ_{em}). The initially excited Franck–Condon state may have a different transition dipole orientation than the emitting state. The rate of vibrational relaxation, k_{vr}, is assumed to be much greater than the rate of internal conversion between the states k_{ba}, k_{ab}. The internal conversion rate is much greater than the radiative and nonradiative rates k_{ar}, k_{br} and k_{anr}, k_{bnr}.

Conclusions

A two-level model for the fluorescence depolarization of tryptophan based on ^1L_a, ^1L_b interconversion kinetics is shown to adequately describe the experimental data. The rate of internal conversion is determined to be (1.6 ps)$^{-1}$. The complex decay

(48) Fischer, G. *Vibronic Coupling*; Academic Press: New York, 1984.
(49) Albrecht, A. C. *J. Mol. Spectrosc.* **1961**, *6*, 84–108.
(50) Wermuth, G.; Rettig, W. *J. Phys. Chem.* **1984**, *88*, 2729–2735.
(51) Orlandi, G.; Siebrand, W. *J. Chem. Phys.* **1973**, *58*, 4513–4523.
(52) Orlandi, G.; Siebrand, W. *Chem. Phys. Lett.* **1972**, *15*, 465–468.
(53) Geldof, P. A.; Rettschnick, R. P. H.; Hoytink, G. J. *Chem. Phys. Lett.* **1971**, *10*, 549–558.
(54) Maroncelli, M.; Fleming, G. R. *J. Chem. Phys.* **1987**, *86*, 6221–6239.
(55) Jarzeba, W.; Walker, G. C.; Johnson, A. E.; Kahlow, M. A.; Barbara, P. F. *J. Phys. Chem.* **1988**, *92*, 7039–7041.

behavior observed in the excitation and emission dependence of the anisotropy decay emphasizes the importance of vibronic coupling between the ^1L_a and ^1L_b electronic manifolds. These results indicate that the use of time-resolved fluorescence depolarization measurements to obtain information on picosecond and subpicosecond librational motions of tryptophan side chains in proteins may be severely complicated by contributions to the anisotropy from electronic and vibronic relaxation processes. Caution must be taken even when long wavelength excitation (>300 nm) is used. For measurements probing motions on time scales longer than about 5-10 ps, however, a time scale separation between electronic and motional depolarization can be assumed. Under these conditions, an "effective" initial anisotropy can be defined and the purely motional behavior of the chromophore analyzed.

As noted earlier by Cross et al.[29] and Chen et al.,[42] the complexity associated with fluorescence anisotropy can be avoided by the use of absorption anisotropy. For measurements of tryptophan motion on a time scale <5 ps absorption anisotropy is clearly the method of choice.

Acknowledgment. This work was supported by grants from the National Science Foundation. We thank Susan Hudson and Joe Beecham for the global analysis programs used in this work and Harry Guttman for his help in their implementation.

Registry No. H-Trp-OH, 73-22-3.

Protonated Nitric Acid. Structure and Relative Stability of Isomeric $H_2NO_3^+$ Ions in the Gas Phase

Fulvio Cacace,*,† Marina Attinà,† Giulia de Petris,† and Maurizio Speranza‡

Contribution from the Università di Roma "La Sapienza", p.le Aldo Moro 5, 00185 Rome, Italy, and Università della Tuscia, via S.C.de Lellis, 01100 Viterbo, Italy. *Received May 31, 1989*

Abstract: Gaseous $H_2NO_3^+$ ions have been obtained from direct protonation of nitric acid by H_3^+, CH_5^+, and H_3O^+ as well as from the protonation of $C_2H_5ONO_2$ followed by C_2H_4 loss. The proton affinity of nitric acid has been estimated to be 168 ± 3 kcal mol^{-1} from the results of bracketing experiments carried out by FT-ICR and CI mass spectrometry. Structural analysis by MIKE and CID spectrometry of $H_2NO_3^+$ ions and of their ^{18}O-labeled isotopomers obtained from the exchange with $H_2{}^{18}O$ provides strong evidence for the existence of two isomers, characterized by the $(HO)_2NO^+$ and the $H_2O{\cdot}NO_2^+$ structure, and for the higher stability of the latter. The results are consistent with those of independent MO SCF calculations, pointing to the higher stability of the $H_2O{\cdot}NO_2^+$ structure.

In a previous communication we have reported preliminary evidence for the existence of two isomeric $H_2NO_3^+$ ions, obtained from the gas-phase protonation of nitric acid and from the protonation-induced loss of ethylene from ethyl nitrate.[1]

We present here a more complete and detailed account of the converging lines of evidence for the existence of isomeric $H_2NO_3^+$ ions in the gas-phase. The experimental techniques employed include the following: (i) chemical ionization (CI) and Fourier transform ion cyclotron resonance (FT-ICR) mass spectrometry, (ii) metastable ion kinetic energy (MIKE) and collisionally induced dissociation (CID) spectrometry, (iii) isotopic exchange of gaseous $H_2NO_3^+$ ions with $H_2{}^{18}O$ and structural characterization of the $H_2NO_2{}^{18}O^+$ species formed.

In the following sections we shall examine the reactions employed for the preparation of $H_2NO_3^+$ ions and their energetics, the closely related problem concerning the proton affinity of gaseous nitric acid, the structural analysis of the $H_2NO_3^+$ ions by MIKE and CID spectrometry, and the relevant aspects of isotopic labeling experiments.

Experimental Section

Materials. He, H_2, CH_4, and C_2H_6 were research purity gases (99.95 mol % minimum purity) from Matheson Gas Products Inc. Deuterium gas, with a stated isotopic purity of 99.7 mol %, was obtained from BOC Spectral Gases Ltd., while ^{18}O-water (98% isotopic purity) was purchased from Cambridge Isotope Laboratories, Inc. The other chemicals were commercially available or were prepared according to established procedures.

Mass Spectrometric Measurements. The CI spectra of HNO_3 and of $EtNO_3$ were recorded with a Hewlett-Packard 5892A quadrupole instrument, measuring the pressure in the CI ion source with a Bourdon-type mechanical gauge.

The measurements were repeated with use of a ZAB-2F magnetic spectrometer (VG Micromass Ltd.), whose CI source was fitted with a MKS Baratron Model 221A capacitance manometer. Typical operating conditions were as follows: electron current 0.5-1.0 mA, electron energy 50 eV, repeller voltage 0 V, source temperature 180 °C, accelerating voltage 8 kV, source inlet temperature 30 °C, and total pressure in the ion source 0.2-0.3 Torr. The ZAB-2F instrument was used as well to record MIKE spectra, at a typical mass resolving power of 2×10^3 and energy resolution of 4×10^3.

The CID spectra of the $H_2NO_3^+$ and $HDNO_3^+$ ions were taken by admitting He into the collision cell of the ZAB-2F spectrometer and increasing the pressure to ca. 10^{-6} Torr, which caused a 30% reduction of the main beam.

The PA of HNO_3 was measured with the "bracketing" technique, in a pressure range of $1-5 \times 10^{-7}$ Torr, at 30 °C, in a Nicolet FT-MS 1000 ICR mass spectrometer equipped with a 2-T superconducting magnet and a 2.54 cm^3 cell.

Results

Preparation of Gaseous $H_2NO_3^+$ Ions. The gas-phase reaction

$$HNO_3 + AH^+ \rightarrow \underset{\mathbf{1}}{H_2NO_3^+} + A \qquad (1)$$

has previously been observed in a particular case, A = H_2O, in flowing-afterglow studies.[2,3] We have unequivocally established the occurrence of proton transfer (1) from various Brønsted acids by triple-resonance experiments carried out at room temperature, at pressures in the range of 10^{-7} Torr, by FT-ICR spectrometry. The results show that ions **1**, irrespective of the protonating agent

(1) Cacace, F.; Attinà, M.; de Petris, G.; Speranza, M. *J. Am. Chem. Soc.* **1989**, *111*, 5481.

(2) Fehsenfeld, F. C.; Ferguson, E. E. *J. Chem. Phys.* **1973**, *59*, 6272.

(3) Fehsenfeld, F. C.; Howard, C. J.; Schmeltekopf, A. L. *J. Chem. Phys.* **1975**, *63*, 2835.

0002-7863/90/1512-1014$02.50/0